Parity-odd multipoles, magnetic charges, and chirality in hematite α-Fe_2O_3

S. W. Lovesey
ISIS Facility & Diamond Light Source, Ltd., Oxfordshire OX11 0QX, United Kingdom

A. Rodríguez-Fernández and J. A. Blanco
Departamento de Física, Universidad de Oviedo, E–33007 Oviedo, Spain

(Received 8 October 2010; published 23 February 2011)

Collinear and canted magnetic motifs in hematite were investigated by J. Kokubun *et al.* [Phys. Rev. B **78**, 115112 (2008)] using x-ray Bragg diffraction magnified at the iron K-edge, and analyses of observations led to various potentially interesting conclusions. We demonstrate that the reported analyses for both nonresonant and resonant magnetic diffraction at low energies near the absorption K-edge are not appropriate. In its place, we apply a radically different formulation, thoroughly tried and tested, that incorporates all magnetic contributions to resonant x-ray diffraction allowed by the established chemical and magnetic structures. Essential to a correct formulation of diffraction by a magnetic crystal with resonant ions at sites that are not centers of inversion symmetry are parity-odd atomic multipoles, time-even (polar) and time-odd (magneto-electric), that arise from enhancement by the electric-dipole ($E1$)–electric-quadrupole ($E2$) event. Analyses of azimuthal-angle scans on two space-group forbidden reflections, hexagonal $(0,0,3)_h$ and $(0,0,9)_h$, collected by Kokubun *et al.* [Phys. Rev. B 78, 115112 (2008)] above and below the Morin temperature ($T_M = 250$ K), allow us to obtain good estimates of contributing polar and magnetoelectric multipoles, including the iron anapole. We show, beyond reasonable doubt, that available data are inconsistent with parity-even events only ($E1$-$E1$ and $E2$-$E2$). For future experiments, we show that chiral states of hematite couple to circular polarization and differentiate $E1$-$E2$ and $E2$-$E2$ events, while the collinear motif supports magnetic charges.

DOI: 10.1103/PhysRevB.83.054427 PACS number(s): 75.50.Ee, 78.70.Ck, 78.20.Ek, 75.47.Lx

I. INTRODUCTION

Enigmas about ichor-like hematite (α-Fe_2O_3) and famed lodestone, both true and some embroidered, have been worried and written about from the time of Greek texts in 315 BC to William Gilbert of Colchester, the father of magnetism, in the 16th century, to Dzyaloshinsky in 1958 who gave a phenomenological theory of weak ferromagnetism. Hematite is the iron sesquioxide that crystallizes into the corundum structure (centrosymmetric space group 167, $R\bar{3}c$) in which ferric (Fe^{3+}, $3d^5$) ions occupy sites 4(c) on the trigonal c axis that are not centers of inversion symmetry. For an extensive review of the history and properties of hematite see, for example, Morrish[1] and Catti *et al.*[2]

At room temperature, the motif of magnetic moments is canted antiferromagnetism with moments in a (basal) plane normal to the c axis. Weak ferromagnetism parallel to a diad axis of rotation symmetry, normal to a mirror plane of symmetry that contains the c axis, is created by a Dzyaloshinsky[3]–Moriya[4] antisymetric interaction $\mathbf{D} \cdot (\mathbf{S_1} \times \mathbf{S_2})$ between spins $\mathbf{S_1}$ and $\mathbf{S_2}$ and the vector $\mathbf{D}$ is parallel to the c axis. The Morin temperature 250 K, at which moments rotate out of the the basal plane to the c axis, may be determined from the temperature dependence of magnetic Bragg peaks observed by neutron diffraction. Rotation of the moments takes place in a range of 10 K in pure crystals but the interval can be much larger, ≈150 K, in mixed materials.[5] Ultimately, moments align with the c axis and create a fully compensating, collinear antiferromagnet with an iron magnetic moment of 4.9 μ_B at 77 K. We follow Dzyaloshinsky[3] and label collinear (low-temperature phase) and canted (room-temperature phase) antiferromagnetism as phases I and II, respectively (see Fig. 1). In phase I hematite is not magnetoelectric unlike eskolaite (Cr_2O_3), which also possesses the corundum structure and collinear antiferromagnetism.

Finkelstein *et al.*[6] and Kokubun *et al.*[7] studied hematite by x-ray Bragg diffraction, with Bragg intensities enhanced by tuning the energy of the primary x-rays to the iron K-absorption edge. In these experiments, attention is given to Bragg reflections that are forbidden by extinction rules for the space group. Often called Templeton and Templeton reflections,[8] the reflections in question are relatively weak and arise from angular anisotropy of valence states that accept the photoejected electron. Following rotation of the crystal about a Bragg wave-vector aligned with the c axis, Finkelstein *et al.*[6] observed a near sixfold periodicity of the intensity that is traced to a triad axis of rotation symmetry that passes through sites occupied by resonant, ferric ions. In general by measuring intensities, collected at space-forbidden reflections, we can obtain information of high-order multipoles existing in the materials such as magnetic charge (or magnetic monopole),[9] electric dipole,[10] anapole,[11,12] quadropole,[13] octupole,[14,15] and hexadecapole.[16,17] Therefore, these weak reflections are extremely sensitive to charge, orbital, and spin electron degrees of freedom and hematite is no exception.[18]

We apply an atomic theory of resonant Bragg diffraction formulated for the corundum structure[19] to data gathered by Kokubun *et al.*[7] at forbidden reflections $(0,0,l)_h$ with $l = 3(2n + 1)$ and infer from available data relative values of atomic multipoles of the resonant ion. A successful story emerges with scattering represented by a mixture of parity-even and parity-odd (even or odd with respect to the inversion of space) multipoles at sites in the structure

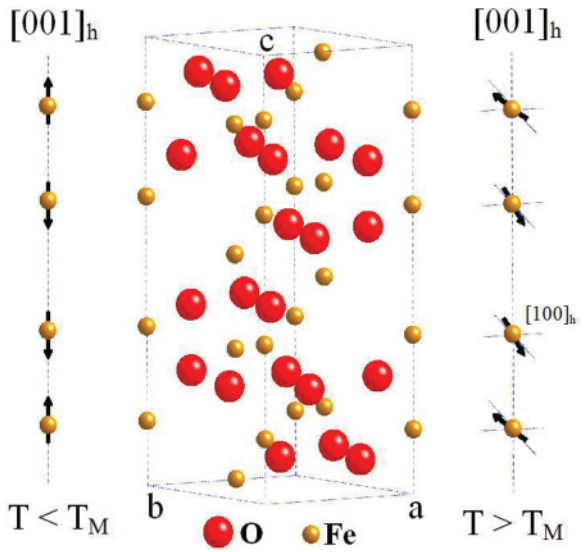

FIG. 1. (Color online) Magnetic and chemical structure of hematite, space group $R\bar{3}c$. The red (large) and the yellow (small) dots represent oxygen and iron sites, respectively. The left line denotes the magnetic motif along the c axis below the Morin temperature (phase I). The right line denotes the motif above the Morin temperature, where iron moments are contained in the a-b plane (phase II).

occupied by resonant iron ions, which are not centers of inversion symmetry. Parity-odd multipoles arise in a resonant event using the electric dipole ($E1$) and electric quadrupole ($E2$)—corresponding multipoles are labeled polar (time-even) or magnetoelectric (time-odd)—while parity-even multipoles arise from $E1$-$E1$ and $E2$-$E2$ events. A chiral state of hematite is demonstrated by a predicted coupling of resonant intensity to circular polarization (helicity) in the primary beam, and the effect also differentiates between $E1$-$E2$ and $E2$-$E2$ events. The two parity-odd multipoles of rank zero correspond to chirality and magnetic charge[20,21] and both pseudoscalar monopoles are present in the electric dipole–magnetic dipole ($E1$-$M1$) amplitude for resonant scattering by hematite in phase I.

Our article is arranged as follows. Section II contains essential information and definitions. Unit-cell structure factors for Bragg diffraction enhanced by $E1$-$E1$, $E1$-$E2$, and $E2$-$E2$ listed in the Appendix are exploited in Secs. III and IV, which report the successful analysis of Bragg diffraction data gathered on hematite at room temperature and at 150 K, well below the Morin transition. Thereafter, in Sec. V, there are simulations of resonant intensity induced by circular polarization in the primary x-ray beam which signals the existence of a chiral state. Section VI addresses the magnetic charge found in the $E1$-$M1$ structure factor and not visible in a dichroic signal. A discussion of findings in Sec. VII concludes the article.

II. BASICS

There are four contributions to the amplitude of photons scattered by electrons calculated in the first level of approximation in the small quantity (E/mc^2), where E is the energy of the primary photon, namely, Thomson scattering, spin scattering, and two contributions with virtual intermediate states, one of which may become large when E coincides with an atomic resonance. Of particular interest with magnetic samples is a celebrated reduction of the amplitude, derived by De Bergevin and Brunel,[22] which occurs at large E. In this limit, all three contributions excluding Thomson scattering add to give so-called magnetic, nonresonant scattering made up simply of spin and orbital magnetic moments. De Bergevin and Brunel's result is not valid at low energies, and certainly not below an atomic resonance, as is at once obvious from the steps in its derivation.[23]

In an analysis of x-ray Bragg diffraction data for hematite collected at space-group forbidden reflections we use the spin and resonant contributions to the scattering amplitude. The spin contribution $G^s = i(E/mc^2)(\mathbf{e}\times\mathbf{e}')\cdot F_s(k)$ with $\mathbf{k} = \mathbf{q}-\mathbf{q}'$, where $\mathbf{e}$ and $\mathbf{q}$ ($\mathbf{e}'$ and $\mathbf{q}'$) are, respectively, the polarization vector and the wave vector of the primary (secondary) photon, and the Bragg angle θ that appears in structure factors for resonant scattering is defined by $\mathbf{q}\cdot\mathbf{q}' = q^2\cos(2\theta)$. $F_s(k)$ is the unit-cell structure factor for spin magnetic moments. The measured energy profiles of reflections $(0,0,3)_h$ and $(0,0,9)_h$ show a single resonance in the pre-edge region, devoid of secondary structure, which is modeled by a single oscillator centered at an energy $\Delta = 7.105$ keV with a width Γ, to an excellent approximation.[7] In this instance, the resonant contribution to scattering is represented by $d(E)F_{\mu'\nu}$, where $d(E) = \Delta/[E-\Delta+i\Gamma]$ and $F_{\mu'\nu}$ is a unit-cell structure factor for states of polarization μ' (secondary) and ν (primary). We follow the standard convention for orthogonal polarization labels σ and π: σ normal to the plane of scattering and, consequently, π in the plane. Unit-cell structure factors listed in the Appendix are derived following steps for the corundum structure found in Lovesey *et al.*[19] The generic form of our Bragg scattering amplitude for hematite at a space-group forbidden reflection (no Thomson scattering) is

$$G_{\mu'\nu}(E) = G^s_{\mu'\nu} + \rho\, d(E)\, F_{\mu'\nu}, \tag{1}$$

where ρ is a collection of factors, which include radial integrals for particular resonance events, which are provided in the Appendix.

Atomic multipoles $\langle T^K_Q\rangle$ in parity-even structure factors, for $E1$-$E1$ and $E2$-$E2$ events, have the property that even rank K are time-even (charge) and odd rank K are time-odd (magnetic). For enhancement at the K-absorption edge, all parity-even atomic multipoles relate to orbital degrees of freedom in the valence shell - spin degrees of freedom are absent.[24] Thus, for enhancement at the K-absorption edge, multipoles $\langle T^K_Q\rangle$ with odd K are zero if the ferric, $3d^5$ (electron configuration ^{6}S) of the iron ion is fully preserved in hematite. The measured iron magnetic moment of 4.9 μ_B at 77 K indicates that the orbital magnetic moment is small and likely no more than $\approx$2% of the measured moment.[2,5]

It is worth noting that we have used a single-domain approach for calculating the intensities, as is mentioned in the penultimate paragraph in Sec. IV D of Kokubun *et al.*[7] The justification is that the x-ray beam was sufficiently small to illuminate only one crystal domain of hematite.

III. PHASE I

We report first our analyses of data gathered by Kokubun *et al.*[7] on hematite at 150 K. With 100% incident σ polarization and no analysis of polarization in the secondary beam, the measured intensity of a Bragg reflection is proportional to

$$I = |G_{\sigma'\sigma}(E)|^2 + |G_{\pi'\sigma}(E)|^2. \quad (2)$$

For a collinear antiferromagnet, in expression (1) for $G_{\mu'\nu}(E)$ one has $G^s_{\sigma'\sigma} = 0$ and in the channel with rotated polarization

$$G^s_{\pi'\sigma} = 4\sin(\theta)\sin(\varphi l)(E/mc^2) f_s(k)\langle S^z\rangle, \quad (3)$$

where $\varphi = -37.91^\circ$, the Bragg angle $\theta = 10.96^\circ$ (34.77°) for a Miller index $l = 3$ (9), $\langle S^z\rangle \leqslant 5/2$ is the spin moment, and $f_s(k)$ is the spin form factor with $f_s(0) = 1$. Note that $|G^s_{\pi'\sigma}|^2 \propto \sin^2(\theta)$ above is not the expression in Eq. (20) in Ref. 7, which is derived by the use of an abridged scattering amplitude that is not valid in the experiment.[22]

At resonance, the spin contribution $G^s_{\pi'\sigma}$ is suppressed compared to the resonant contribution by a factor $\Gamma/\Delta \approx 10^{-4}$ and it may safely be neglected.

Confrontations between our theoretical expressions for the azimuthal-angle dependence of Bragg intensity with the corresponding experimental data reported in Ref. 7 reveal a 30° mismatch of origins in the azimuthal angle. Our origin $\psi = 0$ has the a axis normal to the plane of scattering,[19] whereas Kokubun *et al.*[7] specify an origin such that the a axis is parallel to $\mathbf{q} + \mathbf{q}'$, giving a nominal mismatch in the origin of ψ, between theory and experiment, of 90°. The actual mismatch, 30°, revealed by our analysis of data is likely to arise in the experiments by mistakenly using for reference a basal plane Bragg reflection offset by 60°. In this and the following section we reproduce data as a function of ψ offset by 30° compared to data reported in Figs. 5 and 10 in Ref. 7.

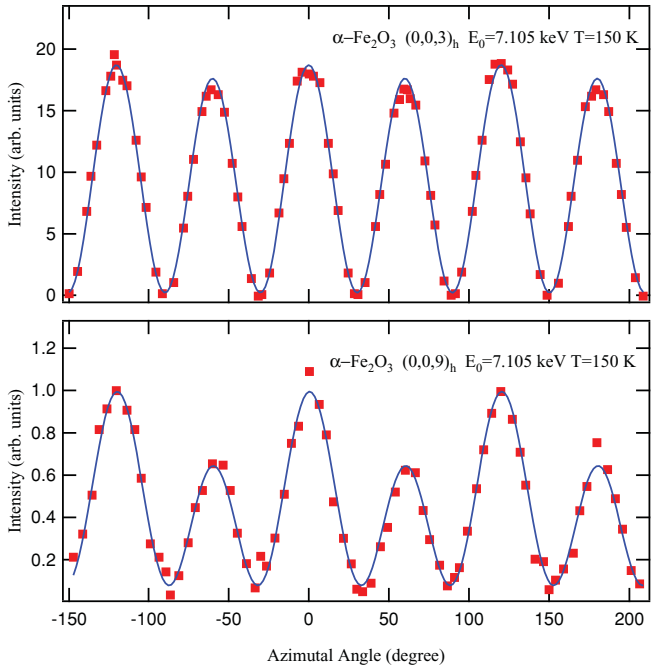

FIG. 2. (Color online) Azimuthal-angle dependence of intensity of Bragg reflections $(0,0,l)_h$ with $l = 3$ and $l = 9$ for phase I (150 K). Continuous curves are fits to structure factors for $E1$-$E2$ and $E2$-$E2$ events with magnetic (time-odd) parity-even multipoles set to zero. Inferred relative atomic multipoles are listed in Table I. Experimental data are taken from Kokubun *et al.*[7]

In light of the established negligible orbital magnetism in hematite, parity-even, time-odd atomic multipoles ($K = 1$ and 3) are set equal to zero. Looking in the Appendix one finds $F_{\mu'\nu}(E1\text{-}E1) = 0$. Additionally, $F_{\sigma'\sigma}(E2\text{-}E2) = 0$ and $F_{\pi'\sigma}(E2\text{-}E2)$ produce Templeton–Templeton scattering proportional to $[\langle T^4_{+3}\rangle' \cos(3\psi)]$, where ψ is the azimuthal angle. Inspection of data for phase I reproduced in Fig. 2 shows that an $E2$-$E2$ event on its own is not an adequate representation. The missing modulation is produced by the $E1$-$E2$ event that introduces a polar quadrupole $\langle U^2_0\rangle$ in phase with the parity-even hexadecapole.[25] Figure 2 displays satisfactory fits of $\{|F_{\sigma'\sigma}|^2 + |F_{\pi'\sigma}|^2\}$, using equal measures of $E1$-$E2$ and $E2$-$E2$ events, to data from azimuthal-angle scans performed at reflections $(0,0,l)_h$ with $l = 3$ and 9. The influence of the polar quadrupole is very notable for $l = 9$ because for this Miller index the hexadecapole is suppressed, with the ratio at $l = 9$ to $l = 3$ of $\tan(\varphi l)$ equal to 0.15. Relative values of multipoles inferred from fits to the low-temperature data are gathered in Table I. Values of $\langle T^4_{+3}\rangle'$ and $\langle U^2_0\rangle$ in phase I are found to be of one sign and in the ratio 20 : 1, with near equal magnitudes of the polar quadrupole and magnetoelectric octupole, $\langle G^3_{+3}\rangle'$. If $|\rho(E2\text{-}E2)/\rho(E1\text{-}E2)| \approx 1.0$, as suggested by our estimate, magnetoelectric multipoles are $\approx$5% of the dominant parity-even hexadecapole, $\langle T^4_{+3}\rangle'$.

Without polarization analysis, it does not seem possible from azimuthal-angle scans to distinguish between $E1$-$E2$ and $E2$-$E2$ events.However, as shown in Sec. V, the two events can be distinguished with circularly polarized x rays.

TABLE I. Relative values of atomic multipoles for collinear antiferromagnetism in phase I (at $\approx$100 K below the Morin transition) and canted antiferromagnetism in phase II (room temperature). Apart from a scale factor, the magnitude of the dominant hexadecapole, $\langle T^4_{+3}\rangle'$, is set to $+10.00$. The estimate $\langle U^2_0\rangle = +0.50$ inferred by fits to data for phase I is also used in the analysis of data for phase II. Values for other multipoles are inferred by fitting to data equal measures of $E1$-$E2$ and $E2$-$E2$ structure factors listed in the Appendix, with time-odd figures (magnetic) multipoles in $E2$-$E2$ set to zero. Fits are displayed in Figs. 2 and 4. With our definition, real $\langle\cdots\rangle'$ and imaginary $\langle\cdots\rangle''$ parts of a multipole are defined through $\langle G^K_Q\rangle = \langle G^K_Q\rangle' + i\langle G^K_Q\rangle''$ with $\langle G^K_Q\rangle^* = (-1)^Q\langle G^K_{-Q}\rangle$, and identical relations for the other two multipoles, $\langle T^K_Q\rangle$ and $\langle U^K_Q\rangle$. All multipoles with projection $Q = 0$ are purely real. Using radial integrals from an atomic code factors in Eq. (1) are in the ratio $\rho(E2\text{-}E2)/\rho(E1\text{-}E2) \approx -0.98$, which is no more than a guide to the actual value in hematite. This ratio is not eliminated in the listed values of the multipoles.

Multipole	Phase I	Phase II
$\langle G^1_{+1}\rangle'$		0.50(2)
$\langle G^2_0\rangle$	0.11(2)	
$\langle G^2_{+1}\rangle''$		−0.38(3)
$\langle G^3_{+1}\rangle'$		1.07(6)
$\langle G^3_{+3}\rangle'$	0.41(2)	2.45(5)

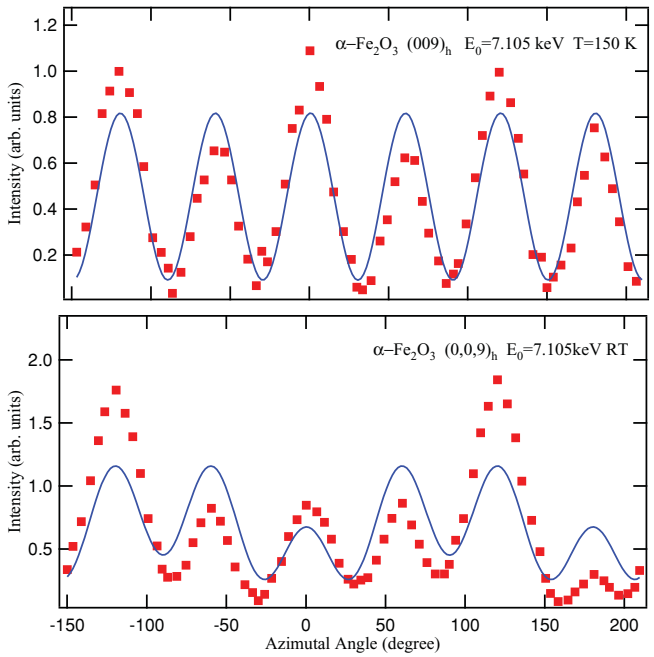

FIG. 3. (Color online) Azimuthal-angle dependence of intensity of the Bragg reflection $(0,0,9)_h$ for phases I (150 K) and II (room temperature). Continuous curves are fits to parity-even structure factors $E1$-$E1$ and $E2$-$E2$ including all magnetic multipoles. Experimental data taken from Kokubun *et al.*[7] appear also in Figs. 2 and 4.

The failure of pure parity-even structure factors $E1$-$E1$ plus $E2$-$E2$ to explain the data is most pronounced for $l = 9$. To illustrate the extent of the failure, Fig. 3 displays a fit to intensity at $l = 9$ with an amplitude made of equal amounts of $E1$-$E1$ and $E2$-$E2$ unit-cell structure factors, and the quality of the fit is clearly inferior to the one shown in Fig. 2.

IV. PHASE II

In this phase, above the Morin transition, iron magnetic moments lie in a plane normal to the c axis. We choose orthonormal principal axes (x, y, z) with the x and z axes parallel to the crystal a and c axes, respectively. The crystal a axis is parallel to a diad axis of rotation symmetry, normal to the mirror plane that contains the trigonal c axis.

The spin contribution $G^s_{\sigma'\sigma} = 0$, while the corresponding $\pi'\sigma$ scattering amplitude can be different from zero and, notably, it depends on the azimuthal angle. We find that

$$G^s_{\pi'\sigma} = 4\cos(\psi)\cos(\theta)\sin(\varphi l)\,(E/mc^2)\,f_s(k)\,\langle S^y\rangle, \quad (4)$$

and $|G^s_{\pi'\sigma}|^2 \propto \cos^2(\theta)$ from Eq. (4) is not the same as the corresponding result, Eq. (19) in Ref. 7 for reasons spelled out in Sec. III.

Away from a resonance, the result (4) predicts a twofold periodicity of intensity as a function of the azimuthal angle, which is in accord with observations in Ref. 7. The spin moment in the mirror plane $\langle S^y\rangle$ is close to 5/2 while spontaneous magnetization, directed along a diad axis, is ≈0.02% of the nominal value. From Eqs. (3) and (4) we see that the ratio of $|G^s_{\pi'\sigma}|^2$ for phases I and II depends on $\tan^2(\theta)$ which takes the value 0.04 (0.48) for $l = 3$ ($l = 9$). For $l = 3$, Kokubun *et al.*[7] report intensity between 150 K (phase I) and 300 K (phase II). Starting from ≈210 K a large increase of intensity is observed over an interval of ≈40 K. Rotation of magnetic moments from the c axis to the basal plane, between phases I and II, takes place in a range of 10 K in pure crystals but the interval can be larger in mixed materials as commented above.

Slightly away from the resonance, interference between the nonresonant, spin contribution (4) and $d(E)F_{\pi'\sigma}$ may enhance intensity in a Bragg peak if $(E-\Delta)[G^s_{\pi'\sigma}/(F_{\pi'\sigma})'] > 0$. We find $[G^s_{\pi'\sigma}/(F_{\pi'\sigma})']$ is of one sign for $l = 3$ and $l = 9$ provided that $f_s(k)$, the spin form factor, is of one sign. At face value this finding is not at one with Kokubun *et al.*[7] who discuss a sighting of slight enhancement of the intensity on the low-energy side of the resonance for $l = 9$ that is apparently absent, or completely negligible, for $l = 3$.

Figure 4 shows fits of $E1$-$E2$ and $E2$-$E2$ structure factors to data gathered at $l = 3$ and $l = 9$ in phase II (room temperature). As before, in our analysis of data gathered on phase I, parity-even multipoles with odd K are set to zero. Time-even contributions to structure factors, determined by chemical structure, are taken to be the same in phases I and II. Consistency with this assumption, about chemical structure, implies for phases I and II the same values of $\langle T^4_{+3}\rangle'$ and $\langle U^2_0\rangle$. Inferred relative values of time-odd atomic multipoles for phase II are listed in Table I, with values of $\langle T^4_{+3}\rangle'$ and $\langle U^2_0\rangle$ in the ratio 20:1. Relative to the magnitude of $\langle U^2_0\rangle$, none of the magnetoelectric multipoles are negligible in phase II. Figure 3 contains a fit of pure parity-even structure factors, $E1$-$E1$ and $E2$-$E2$, to data for the reflection $l = 9$, and the quality of the fit is clearly inferior to that reported in Fig. 4 with $E1$-$E2$ and $E2$-$E2$ structure factors.

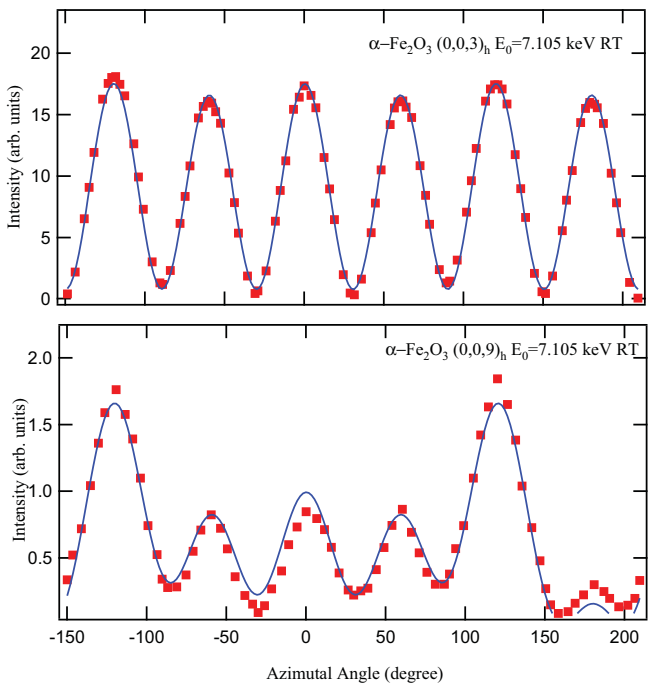

FIG. 4. (Color online) Azimuthal-angle dependence of the intensity of Bragg reflections $(0,0,l)_h$ with $l = 3$ and $l = 9$ for phase II (room temperature). Continuous curves are fits to structure factors for $E1$-$E2$ and $E2$-$E2$ events with magnetic (time-odd) parity-even multipoles set to zero. Inferred relative atomic multipoles are listed in Table I. Experimental data are taken from Kokubun *et al.*[7]

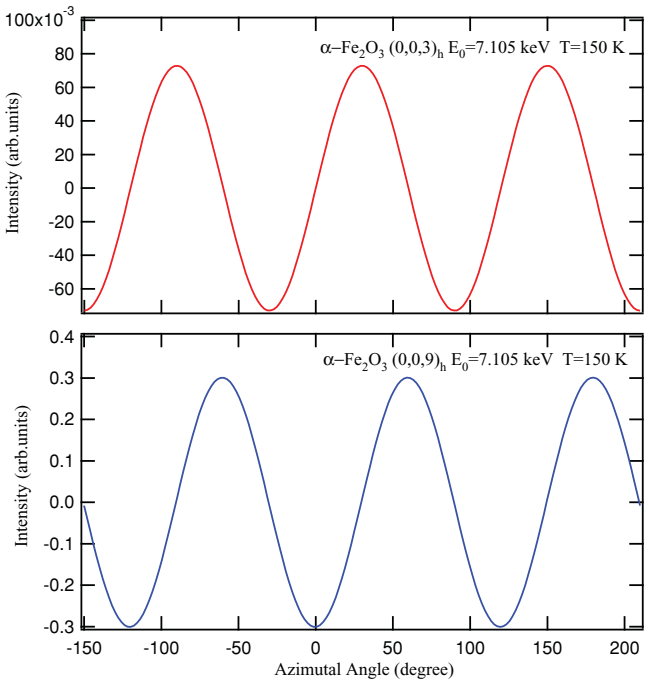

FIG. 5. (Color online) Simulation of the azimuthal-angle dependence from Eq. (6) for a circular polarized light of Bragg reflections $(0,0,l)_h$ with $l = 3$ and $l = 9$ for phase I. Continuous curves are simulations made with the values of the multipoles from the $E1$-$E2$ event gathered in Table I. For the $E2$-$E2$ event I_c is zero because our magnetic (time-odd) parity-even multipoles are zero for a ferric ion. Zero I_c does not mean zero intensity because I_c is only the circular polarization contribution to intensity.[17]

V. CHIRAL STATE

A chiral, or handed, state of a material is permitted to couple to a probe with a like property, in our case circular polarization (helicity) in the primary beam of x rays. In our notation, the pseudoscalar for helicity, P_2, is one of three purely real, time-even Stokes parameters. Intensity induced by helicity in the primary beam is (Ref. 17)

$$I_c = P_2 \mathrm{Im}\{G^*_{\sigma'\pi} G_{\sigma'\sigma} + G^*_{\pi'\pi} G_{\pi'\sigma}\}, \tag{5}$$

where the amplitudes $G_{\mu'\nu}$ are given by Eq. (1) and * denotes complex conjugation. I_c is zero for Thomson scattering since it is proportional to $(\mathbf{e}\cdot\mathbf{e}')$ and diagonal with respect to states of polarization.

Let us consider the fully compensating collinear antiferromagnet (phase I). For both $E1$-$E1$ and $E1$-$M1$ events there are no contributions diagonal with respect to states of polarization and I_c is zero. Using the structure factors listed in the Appendix for the $E1$-$E2$ and $E2$-$E2$ events, we find

$$I_c(E1\text{-}E2) = -P_2\left(\frac{8\sqrt{2}}{5}\right)\rho^2(E1\text{-}E2)\mid d(E)\mid^2 \sin(3\psi) \times \cos^3(\theta)[1+\sin^2(\theta)]\cos^2(\varphi l)\langle G^3_{+3}\rangle'\langle U^2_0\rangle \tag{6}$$

and

$$I_c(E2\text{-}E2) = -P_2 4\rho^2(E2\text{-}E2)\mid d(E)\mid^2 \sin(6\psi) \times \sin(\theta)\cos^6(\theta)\sin^2(\varphi l)\langle T^3_{+3}\rangle''\langle T^4_{+3}\rangle', \tag{7}$$

The predicted intensities are significantly different—notably in dependence on the azimuthal angle—and offer a method by which to distinguish contributions from the two events (see Figs. 5 and 6). Intensities (6) and (7) depend on long-range magnetic order, with $I_c(E2\text{-}E2) = 0$ if the ferric ion is pure ^{6}S. The polar quadrupole in Eq. (6) is a manifestation of local chirality,[19,25] whereas the pseudoscalar $\langle U^0_0\rangle$, discussed in the next section, is a conventional measure of the chirality of a material. While for phase II, we find that I_c is given

$$I_c(E1\text{-}E2) = P_2\left(\frac{8\sqrt{2}}{5}\right)\rho^2(E1\text{-}E2)|d(E)|^2\cos^2(\varphi l)\cos^2(\theta)\langle U^2_0\rangle\left\{\frac{1}{\sqrt{3}}\sin(\psi)\left[\frac{-3}{\sqrt{5}}[\cos(3\theta)+\cos(\theta)]\langle G^1_{+1}\rangle' \times[\cos(3\theta)-\cos(\theta)]\langle G^2_{+1}\rangle'' - \frac{1}{\sqrt{5}}[\cos^3(\theta)+2\cos(\theta)]\langle G^3_{+1}\rangle'\right] - \sin(3\psi)\cos(\theta)[1+\sin^2(\theta)]\langle G^3_{+3}\rangle'\right\}, \tag{8}$$

$$I_c(E2\text{-}E2) = -P_2\left(\frac{1}{\sqrt{2}}\right)\rho^2(E2\text{-}E2)|d(E)|^2\sin^2(\varphi l)\langle T^4_{+3}\rangle'\left\{4\sin(\psi)\cos^4(\theta)\left[\frac{-1}{\sqrt{5}}\sin(\theta)[8\cos^2(\theta)-5]\langle T^1_1\rangle'' + \sqrt{\frac{3}{5}}\sin(\theta)\cos^3(\theta)\langle T^3_{+1}\rangle''\right] - 4\sqrt{2}\sin(\theta)\cos^6(\theta)\sin(6\psi)\langle T^3_{+3}\rangle''\right\}. \tag{9}$$

VI. MAGNETIC CHARGE AND CHIRALITY

The pseudoscalar monopoles $\langle G^0_0\rangle$ and $\langle U^0_0\rangle$ have particularly simple and interesting physical interpretations. Both monopoles are allowed in hematite structure factors for the $E1$-$M1$ event, as we see by inspection of relevant expressions in the Appendix. A conventional measure of the chirality of electrons in a molecule or extended media is $\langle \mathbf{S}\cdot\mathbf{p}\rangle/|\langle\mathbf{p}\rangle|$, where $\mathbf{S}$ and $\mathbf{p}$ are operators for spin and linear momentum and, not unsurprisingly, $\langle U^0_0\rangle$ is proportional to $\langle \mathbf{S}\cdot\mathbf{p}\rangle/|\mathbf{p}|$. It is well-known that $\langle U^0_0\rangle$ contributes to natural circular dichroism.[26] On the other hand, $\langle G^0_0\rangle$, a magnetic charge,

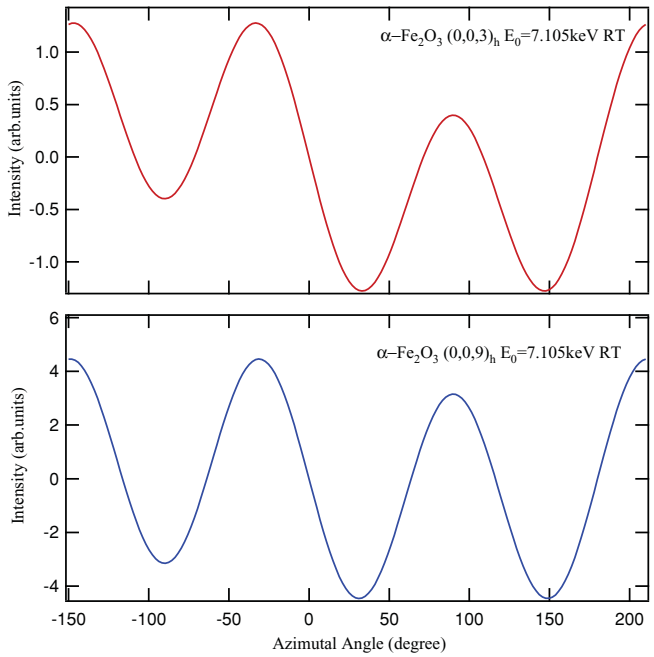

FIG. 6. (Color online) Simulation of the azimuthal-angle dependence from Eq. (8) for a circular polarized light of Bragg reflections $(0,0,l)_h$ with $l = 3$ and $l = 9$ for phase II (room temperature). Continuous curves are simulations made with the values of the multipoles from the $E1$-$E2$ event gathered in Table I. For the $E2$-$E2$ event the I_c is equal to zero because our magnetic (time-odd) parity-even multipoles are zero. Zero I_c does not mean zero intensity since I_c is only the circular polarization contribution.[17]

does not contribute to dichroic signals but it can contribute in scattering. Such is the case for gallium ferrate[27] and phase I of hematite. The magnetic charge and the magnetoelectric quadrupole are present in the amplitude for backscattering with $\mathbf{q} = -\mathbf{q}'$.

VII. DISCUSSION

We report successful analyses of resonant Bragg diffraction data gathered by Kokubun *et al.*[7] on hematite in the collinear (phase I) and canted (phase II) antiferromagnetic phases, with no analysis of diffraction according to polarization of the x rays. We infer good estimates of iron atomic multipoles and find large amounts of parity-odd multipoles. Of particular importance to a successful analysis is a polar quadrupole, a measure of local chirality,[25] and, in phase II, magnetoelectric multipoles that include the anapole. Slight departures between our theory and experiment could be due to a less than ideal crystal, as witnessed in the extended interval of temperature for rotation of magnetic moments between phases I and II.[7]

Future experiments might employ polarization analysis that will allow closer scrutiny of the unit-cell structure factors for hematite that we list in the Appendix, which are derived from the established chemical and magnetic structures of hematite. We predict for phase I that scattering enhanced by the $E1$-$M1$ event contains monopoles that represent chirality and magnetic charge.

Our analyses of data are based on an atomic theory of x-ray Bragg diffraction[19] with unit-cell structure factors that are fundamentally different from the corresponding structure factors employed by Kokubun *et al.*[7] One difference arises in the treatment of nonresonant magnetic scattering. We use the exact expression, due solely to spin moments, while Kokubun *et al.*[7] mistakenly—because it is not valid in the investigated interval of energy—use an abridged amplitude by de Bergevin and Brunel[22] that is a sum of the exact expression and the high-energy limit of two contributions to scattering that involve intermediate states (one of the two is capable of showing a resonance). Treating the resonance as a single oscillator, in accord with the reported energy profile, our structure factors for resonant diffraction are completely determined with no arbitrary phase factors, unlike the analysis in Ref. 7. This difference in the analyses is a likely explanation of our evidence that published data for azimuthal-angle scans are miss-set by 30°. Our treatment of magnetic (time-odd) contributions to scattering is another major difference in the analyses. Whereas Kokubun *et al.*[7] allow only the dipole in the $E1$-$E1$ event we consider all permitted time-odd contributions in both parity-even and parity-odd events. Time-odd multipoles from parity-even events, $\langle T^K_Q \rangle$ with odd K, are related to orbital magnetism when the intermediate state in resonance is an s state, as is the case in the experiments in question with absorption at the iron K-edge. The available evidence is that orbital magnetism of the ferric ion in hematite is negligible, as expected for an s-state ion, and the same can be said of the parity-even, time-odd multipoles, including the dipole which at resonance is the only source of magnetic scattering considered in Ref. 7. From our analysis, we conclude that magnetic scattering at resonance is provided by magnetoelectric multipoles in an $E1$-$E2$ event. We demonstrate beyond reasonable doubt that allowing magnetic $\langle T^K_Q \rangle$ different from zero the available data are not consistent with diffraction enhanced by purely parity-even events, $E1$-$E1$ and $E2$-$E2$.

In summary, we have derived information on the relative magnitude of multipoles for the antiferromagnetic phases of hematite (above and below the Morin temperature). These estimates are obtained from analyses of experimental azimuthal dependence gathered in resonant x-ray Bragg diffraction at space-group forbidden reflections $(0,0,3)_h$ and $(0,0,9)_h$. A chiral electron state is proposed from a predicted coupling of resonant intensity to circular polarization in the primary beam. This effect allows differentiating between contributions of the $E1$-$E2$ and $E2$-$E2$ events. In addition, pseudoscalar monopoles (chirality and magnetic charge) are present in the $E1$-$M1$ amplitude for resonant scattering by hematite below the Morin temperature.

ACKNOWLEDGMENTS

Gerrit van der Laan provided values of atomic radial integrals for a ferric ion. We have benefited from discussions with A. Bombardi and S. P. Collins and correspondence with F. de Bergevin. S.W.L is grateful to E. Balcar for ongoing noetic support. Financial support has been received from Spanish FEDER-MiCiNN Grant No. Mat2008-06542-C04-03. A.R.F is grateful to Gobierno del Principado de Asturias for the financial support from Plan de Ciencia, Tecnología e Innovación (PTCI) de Asturias.

APPENDIX: UNIT-CELL STRUCTURE FACTORS

Some factors in Eq. (1) contain a dimensionless quantity $\aleph = m\Delta a_0^2/\hbar^2 = 260.93$, where a_0 is the Bohr radius and $\Delta = 7.105$ keV. Radial integrals for the $E1$ and $E2$ processes at the K-absorption edge are denoted by $\{R\}_{sp}$ and $\{R^2\}_{sd}$. Estimates from an atomic code are $\{R\}_{1s4p}/a_0 = -0.0035$ and $\{R^2\}_{1s3d}/a_0^2 = 0.00095$, and it is interesting that the magnitudes are smaller than hydrogenic values with $Z = 26$ by a factor of about 3. More appropriate values of the radial integrals will be influenced by ligand ions. The $M1$ process between stationary states of an isolated nonrelativistic ion is forbidden because the radial overlap of initial and final states in the process is zero, on account of orthogonality. For an $M1$ process in a compound the radial integral, denoted here by $\{1\}_{\gamma\gamma}$, is an overlap of two orbitals with common orbital angular momentum, Γ, which may be centered on different ions. The magnitude of $\{1\}_{\gamma\gamma}$ is essentially a measure of configuration interactions and bonding, or covalancy, of a cation and ligands. Factors appearing in Eq. (1) are

$$\rho(E1\text{-}E1) = [\{R\}_{sp}/a_0]^2\aleph, \tag{A1}$$

$$\rho(E1\text{-}M1) = q\{R\}_{sp}\{1\}_{\gamma\gamma}, \tag{A2}$$

$$\rho(E1\text{-}E2) = \left[q\{R^2\}_{sd}R_{sp}/a_0^2\right]\aleph, \tag{A3}$$

$$\rho(E2\text{-}E2) = [q\{R^2\}_{sd}/a_0]^2\aleph. \tag{A4}$$

Hematite structure factors $F_{\mu'\nu}$ for forbidden reflections $(0,0,l)_h$ with $l = 3(2n+1)$ and enhancements by $E1$-$E1$, $E1$-$M1$, $E1$-$E2$, and $E2$-$E2$ events are listed below. In these expressions, the angle $\varphi = -\pi u$, where $u = 2z - 1/2 = 0.2104$ for α-Fe_2O_3, the angle θ is the Bragg angle, and $\langle T_Q^K\rangle$, $\langle G_Q^K\rangle$, and $\langle U_Q^K\rangle$ are the mean values of the atomic tensors involved.

1. Collinear antiferromagnet, phase I

($E1$-$E1$)

$$F_{\sigma'\sigma}(E1\text{-}E1) = 0 \tag{A5}$$

$$F_{\pi'\sigma}(E1\text{-}E1) = -2\sqrt{2}\sin(\varphi l)\sin(\theta)\langle T_0^1\rangle \tag{A6}$$

$$F_{\pi'\pi}(E1\text{-}E1) = 0 \tag{A7}$$

($E1$-$M1$)

$$F_{\sigma'\sigma}(E1\text{-}M1) = 0 \tag{A8}$$

$$F_{\pi'\sigma}(E1\text{-}M1) = \frac{2\sqrt{2}}{\sqrt{3}}\cos(\varphi l)\left\{2\sqrt{2}\left[-\sin^2(\theta)\langle G_0^0\rangle + i\cos^2(\theta)\langle U_0^0\rangle\right] + [2+\cos^2(\theta)]\langle G_0^2\rangle + i\cos^2(\theta)\langle U_0^2\rangle\right\} \tag{A9}$$

$$F_{\pi'\pi}(E1\text{-}M1) = 0 \tag{A10}$$

($E1$-$E2$)

$$F_{\sigma'\sigma}(E1\text{-}E2) = -\frac{4\sqrt{2}}{\sqrt{5}}\sin(3\psi)\cos(\varphi l)\cos(\theta)\langle G_{+3}^3\rangle' \tag{A11}$$

$$F_{\pi'\sigma}(E1\text{-}E2) = \frac{2}{\sqrt{5}}\cos(\varphi l)\left\{-[3\cos^2(\theta)-2]\langle G_0^2\rangle + i\cos^2(\theta)\langle U_0^2\rangle - \sqrt{2}\sin(2\theta)\cos(3\psi)\langle G_{+3}^3\rangle'\right\} \tag{A12}$$

$$F_{\pi'\pi}(E1\text{-}E2) = -\frac{4\sqrt{2}}{\sqrt{5}}\sin(3\psi)\cos(\varphi l)\cos(\theta)\sin^2(\theta)\langle G_{+3}^3\rangle' \tag{A13}$$

($E2$-$E2$)

$$F_{\sigma'\sigma}(E2\text{-}E2) = -\sqrt{2}\sin(3\psi)\sin(\varphi l)\langle T_{+3}^3\rangle'' \tag{A14}$$

$$F_{\pi'\sigma}(E2\text{-}E2) = \sqrt{\frac{2}{5}}\sin(\varphi l)\left\{\sin(3\theta)\langle T_0^1\rangle - \sin(\theta)[3\cos^2(\theta)-2]\langle T_0^3\rangle - \frac{\sqrt{5}}{4}\cos(3\psi)\left[[3\cos(3\theta)+\cos(\theta)]\langle T_{+3}^3\rangle'' - i[\cos(3\theta)+3\cos(\theta)]\langle T_{+3}^4\rangle'\right]\right\} \tag{A15}$$

$$F_{\pi'\pi}(E2\text{-}E2) = -\frac{1}{\sqrt{2}}\sin(3\psi)\sin(\varphi l)\sin(4\theta)\langle T_{+3}^3\rangle'' \tag{A16}$$

2. Canted antiferromagnet, phase II

Time-even contributions to structure factors, determined by chemical structure, are the same in phases I and II. Thus the structure factor with polar multipoles, $F_{\mu'\nu}(u)$, for phase II is identical to the foregoing expression for phase I. For the convenience of the reader, structure factors for parity-even multipoles, $F_{\mu'\nu}(t)$, are given in full, although only contributions with $K = 1$ and 3 differ from foregoing expressions.

($E1$-$E1$)

$$F_{\sigma'\sigma}(E1\text{-}E1) = 0 \tag{A17}$$

$$F_{\pi'\sigma}(E1\text{-}E1) = 4\cos(\psi)\sin(\varphi l)\cos(\theta)\langle T_{+1}^1\rangle'' \tag{A18}$$

$$F_{\pi'\pi}(E1\text{-}E1) = 4\sin(\psi)\sin(\varphi l)\sin(2\theta)\langle T_{+1}^1\rangle'' \tag{A19}$$

($E1$-$M1$)

$$F_{\sigma'\sigma}(E1\text{-}M1) = 8\sin(\psi)\cos(\varphi l)\cos(\theta)\left[-\langle G_{+1}^1\rangle' + \langle G_{+1}^2\rangle''\right] \tag{A20}$$

$$F_{\pi'\sigma}(E1\text{-}M1) = 4\cos(\psi)\cos(\varphi l)\sin(2\theta)\left[\langle G_{+1}^1\rangle\right] \tag{A21}$$

$$F_{\pi'\pi}(E1\text{-}M1) = -8\sin(\psi)\cos(\varphi l)\cos(\theta)\left[\langle G_{+1}^1\rangle' + \langle G_{+1}^2\rangle''\right] \tag{A22}$$

($E1$-$E2$)

$$F_{\sigma'\sigma}(E1\text{-}E2) = \frac{4\sqrt{2}}{\sqrt{5}}\cos(\varphi l)\cos(\theta)\left\{\frac{1}{\sqrt{3}}\sin(\psi)\left[\frac{-3}{\sqrt{5}}\langle G_{+1}^1\rangle' - \langle G_{+1}^2\rangle'' + \frac{1}{\sqrt{5}}\langle G_{+1}^3\rangle'\right] - \sin(3\psi)\langle G_{+3}^3\rangle'\right\} \tag{A23}$$

$$F_{\pi'\sigma}(E1\text{-}E2) = 2\sqrt{\frac{2}{5}}\cos(\varphi l)\sin(2\theta)\left\{\frac{\cos(\psi)}{\sqrt{3}}\left[\frac{3}{\sqrt{5}}\langle G_{+1}^1\rangle' - 2\langle G_{+1}^2\rangle'' - \frac{1}{\sqrt{5}}\langle G_{+1}^3\rangle'\right] - \cos(3\psi)\langle G_{+3}^3\rangle'\right\} \tag{A24}$$

$$F_{\pi'\pi}(E1\text{-}E2) = -\frac{4\sqrt{6}}{5}\cos(\varphi l)\Big\{\sqrt{\frac{5}{3}}\cos(\theta)\sin^2(\theta)\sin(3\psi)\langle G^3_{+3}\rangle' + \sin(\psi)\Big[\cos(3\theta)\Big(\langle G^1_{+1}\rangle' - \frac{\sqrt{5}}{3}\langle G^2_{+1}\rangle''\Big) + \frac{1}{3}\cos(\theta)[\cos^2(\theta)+3]\langle G^3_{+1}\rangle'\Big]\Big\} \quad \text{(A25)}$$

$(E2\text{-}E2)$

$$F_{\sigma'\sigma}(E2\text{-}E2) = \sin(2\theta)\sin(\varphi l)\Big\{\sin(\psi)\Big[\frac{-2}{\sqrt{5}}\langle T^1_{+1}\rangle'' - \sqrt{\frac{6}{5}}\langle T^3_{+1}\rangle''\Big] + \sqrt{2}\sin(3\psi)\langle T^3_{+3}\rangle''\Big\} \quad \text{(A26)}$$

$$F_{\pi'\sigma}(E2\text{-}E2) = -\sin(\varphi l)\Big\{\cos(\psi)\Big[\frac{2}{\sqrt{5}}\cos(3\theta)\langle T^1_{+1}\rangle'' + \sqrt{\frac{6}{5}}\cos(\theta) \times [1+\sin^2(\theta)]\langle T^3_{+1}\rangle''\Big] + \frac{1}{2\sqrt{2}}\cos(3\psi) \times \big[\cos(\theta)[3\cos(3\theta)+\cos(\theta)]\langle T^3_{+3}\rangle''\big]\Big\} \quad \text{(A27)}$$

$$F_{\pi'\pi}(E2\text{-}E2) = \frac{1}{\sqrt{2}}\sin(\varphi l)\sin(4\theta)\Big\{\sin(\psi)\Big[-\frac{4\sqrt{2}}{\sqrt{5}}\langle T^1_{+1}\rangle'' + \sqrt{\frac{3}{5}}\langle T^3_{+1}\rangle''\Big] - \sin(3\psi)\langle T^3_{+3}\rangle''\Big\} \quad \text{(A28)}$$

[1] A. H. Morrish, *Canted Antiferromagnetism: Hematite* (World Scientific, Singapore, 1994).
[2] M. Catti, G. Valerio, and R. Dovesi, Phys. Rev. B **51**, 7441 (1995).
[3] I. Dzyaloshinsky, J. Phys. Chem. Solids **4**, 241 (1958).
[4] T. Moriya, Phys. Rev. **120**, 91 (1960).
[5] E. Krén, P. Szabó, and G. Konczos, Phys. Lett. **19**, 103 (1965).
[6] K. D. Finkelstein, Q. Shen, and S. Shastri, Phys. Rev. Lett. **69**, 1612 (1992).
[7] J. Kokubun, A. Watanabe, M. Uehara, Y. Ninomiya, H. Sawai, N. Momozawa, K. Ishida, and V. E. Dmitrienko, Phys. Rev. B **78**, 115112 (2008).
[8] D. Templeton and L. Templeton, Acta Crystallogr. Sect. A: Cryst. Phys. Diffr. Theor. Gen. Crystallogr. **38**, 62 (1982).
[9] S. W. Lovesey and V. Scagnoli, J. Phys. Condens. Matter **21**, 474214 (2009).
[10] J. Fernández-Rodríguez, J. A. Blanco, P. J. Brown, K. Katsumata, A. Kikkawa, F. Iga, and S. Michimura, Phys. Rev. B **72**, 052407 (2005).
[11] S. W. Lovesey, J. Fernández-Rodríguez, J. A. Blanco, D. S. Sivia, K. S. Knight, and L. Paolasini, Phys. Rev. B **75**, 014409 (2007).
[12] J. Fernández-Rodríguez, V. Scagnoli, C. Mazzoli, F. Fabrizi, S. W. Lovesey, J. A. Blanco, D. S. Sivia, K. S. Knight, F. de Bergevin, and L. Paolasini, Phys. Rev. B **81**, 085107 (2010).
[13] S. B. Wilkins, R. Caciuffo, C. Detlefs, J. Rebizant, E. Colineau, F. Wastin, and G. H. Lander, Phys. Rev. B **73**, 060406 (2006).
[14] J. A. Paixão, C. Detlefs, M. J. Longfield, R. Caciuffo, P. Santini, N. Bernhoeft, J. Rebizant, and G. H. Lander, Phys. Rev. Lett. **89**, 187202 (2002).
[15] S. W. Lovesey and K. S. Knight, J. Phys. Condens. Matter **12**, L367 (2000).
[16] Y. Tanaka, T. Inami, S. W. Lovesey, K. S. Knight, F. Yakhou, D. Mannix, J. Kokubun, M. Kanazawa, K. Ishida, S. Nanao, T. Nakamura, H. Yamauchi, H. Onodera, K. Ohoyama, and Y. Yamaguchi, Phys. Rev. B **69**, 024417 (2004).
[17] J. Fernández-Rodríguez, S. W. Lovesey, and J. A. Blanco, Phys. Rev. B **77**, 094441 (2008).
[18] S. W. Lovesey and K. S. Knight, J. Phys. Condens. Matter **12**, L367 (2000).
[19] S. W. Lovesey, E. Balcar, K. S. Knight, and J. Fernández-Rodríguez, Phys. Rep. **411**, 233 (2005).
[20] S. W. Lovesey and E. Balcar, J. Phys. Soc. Jpn. **79**, 074707 (2010).
[21] S. W. Lovesey and E. Balcar, J. Phys. Soc. Jpn. **79**, 104702 (2010).
[22] F. De Bergevin and M. Brunel, Acta Crystallogr. A **37**, 324 (1981).
[23] S. W. Lovesey, Rep. Prog. Phys. **56**, 257 (1993).
[24] S. W. Lovesey, J. Phys. Condens. Matter **10**, 2505 (1998).
[25] V. E. Dmitrienko and E. N. Ovchinnikova, Acta Crystallogr. A **57**, 642 (2001).
[26] S. P. Collins, S. W. Lovesey, and E. Balcar, J. Phys. Condens. Matter **19**, 213201 (2005).
[27] U. Staub, Y. Bodenthin, C. Piamonteze, M. García-Fernández, V. Scagnoli, M. Garganourakis, S. Koohpayeh, D. Fort, and S. W. Lovesey, Phys. Rev. B **80**, 140410 (2009).